ARTICLES
PUBLISHED ONLINE: 8 SEPTEMBER 2013 | DOI: 10.1038/NPHYS2734
nature physics

# Spontaneous creation of Kibble–Zurek solitons in a Bose–Einstein condensate

Giacomo Lamporesi, Simone Donadello, Simone Serafini, Franco Dalfovo and Gabriele Ferrari*

**When a system crosses a second-order phase transition on a finite timescale, spontaneous symmetry breaking can cause the development of domains with independent order parameters, which then grow and approach each other creating boundary defects. This is known as the Kibble–Zurek mechanism. Originally introduced in cosmology, it applies to both classical and quantum phase transitions, in a wide variety of physical systems. Here we report on the spontaneous creation of solitons in Bose–Einstein condensates through the Kibble–Zurek mechanism. We measure the power-law dependence of defect number on the quench time, and show that lower atomic densities enhance defect formation. These results provide a promising test bed for the determination of critical exponents in Bose–Einstein condensates.**

The Kibble–Zurek mechanism (KZM) describes the spontaneous formation of defects in systems that cross a second-order phase transition at a finite rate[1–5]. The mechanism was first proposed in the context of cosmology to explain how, during the expansion of the early Universe, the rapid cooling below a critical temperature induced a cosmological phase transition resulting in the creation of domain structures. In fact, the KZM is widespread in nature and applies to both classical and quantum phase transitions[6,7]. Experimental evidence has been observed in superfluid $^3$He (refs 8,9), in superconducting films[10] and rings[11–14] and in ion chains[15–17]. Bose–Einstein condensation in trapped cold gases has been considered as an ideal platform for the KZM (refs 18–22); the system is extremely clean and controllable and particularly suitable for the investigation of interesting effects arising from the spatial inhomogeneities induced by the confinement. Quantized vortices produced in a pancake-shaped condensate by a fast quench across the transition temperature have already been observed[23], but their limited statistics prevented a test of the KZM scaling. The KZM has been studied across the quantum superfluid to Mott insulator transition with atomic gases trapped in optical lattices[24,25]. Here we report on the observation of solitons resulting from phase defects of the order parameter, spontaneously created in an elongated Bose–Einstein condensate (BEC) of sodium atoms. We show that the number of solitons in the final condensate grows according to a power law as a function of the rate at which the transition is crossed, consistent with the expectations of the KZM, and provide the first indication of the KZM scaling with the sonic horizon. We support our observations by comparing the estimated speed of the transition front in the gas to the speed of the sonic causal horizon, showing that solitons are produced in a regime of inhomogeneous KZM (refs 5,20,26). Our measurements can open the way to the determination of the critical exponents of the BEC transition in trapped gases, for which so far little information is available[27].

The KZM predicts the formation of independent condensates when the system crosses the BEC transition at a sufficiently fast rate. Further cooling and thermalization below the critical temperature cause the independent condensates to grow. In axially elongated trapping potentials, as in our experiment where the aspect ratio is about 10, neighbouring condensates with different phases will approach, forming planar non-topological solitonic defects[18] (Fig. 1a (i–iii) for a pictorial view). We characterize this process by counting the solitons as a function of the quench time and the atom number at the transition by means of direct imaging after a ballistic expansion of the sample (Fig. 1a (iv–v)). Figure 1b shows a typical density distribution of a condensate with a negligible thermal component after a long time-of-flight (TOF) integrated along one radial direction. In Figure 1c, a clear density depletion is visible and we interpret it as a soliton. More solitons are shown in the other panels, including cases where the solitonic planes are bent and/or collide as in Fig. 1f,g. We never observe structures that could be identified as topological defects such as vortices and vortex rings, which would be favoured in less elongated traps or pancake-shaped condensates[23]. As opposed to artificially created solitons through phase imprinting techniques[28–30] or by exciting the superfluid with laser pulses or through collisions[31,32], our solitons spontaneously form when the BEC is created by crossing the transition temperature.

The identification of these defects as solitons is based on several arguments: they are simultaneously observed as lines from two orthogonal directions in the radial plane, demonstrating their planar structure, mostly perpendicular to the weak axis of confinement; sometimes they exhibit a bent shape as we expect for snake oscillations[33] of soliton planes; when two of these defects overlap, they appear as solitons in a collision[34], whose individual structure is preserved except in the crossing region. Finally their size after TOF is of the right order of magnitude. This can be deduced by considering that the width of a soliton is of the order of the healing length $\xi = (8\pi an)^{-1/2}$, where $a$ is the scattering length and $n$ is the spatial density. One can then assume that, during the initial fast expansion of the gas in the radial direction, the healing length increases by adiabatically following the density reduction, similarly to what happens to the cores of quantized vortices in a disc-shaped condensate subject to a rapid expansion in the axial direction[35]. As a consequence, a long TOF allows for a better visibility and counting resolution. The expansion times we chose for imaging are indeed much longer than standard ones, thanks to an external magnetic field gradient used for levitating the gas against gravity; this is essential to reduce the optical density well below saturation and for solitons to become large enough to be clearly detected.

INO-CNR BEC Center and Dipartimento di Fisica, Università di Trento, 38123 Povo, Italy. *e-mail: ferrari@science.unitn.it

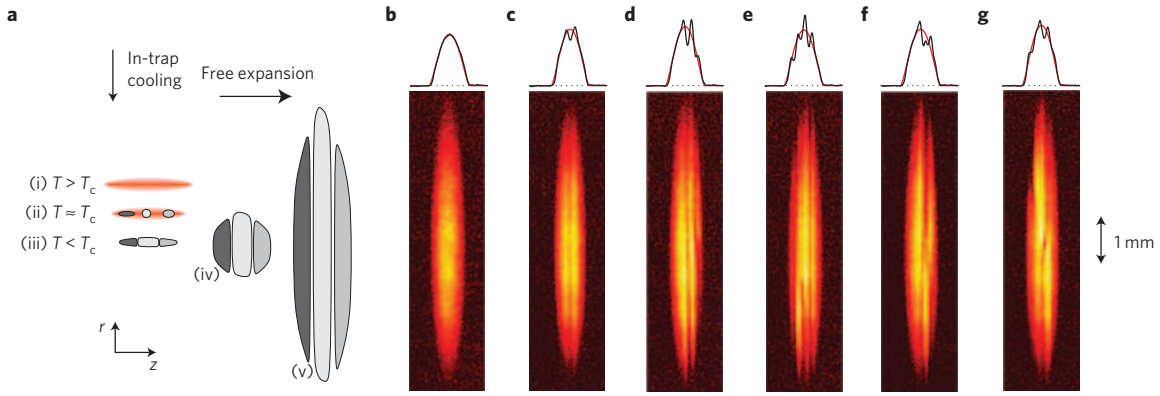


**Figure 1 | Solitons in an elongated BEC. a**, Formation after a quenched cooling of a thermal gas ((i), red) across the BEC transition; BEC is locally achieved forming several isles (ii) each with its own phase (grey). Further cooling makes the isles grow towards each other (iii) forming solitons. The elongated sample is released from the trap and allowed to expand for 180 ms in a levitating field, acquiring a pancake shape (iv, v). **b**–**g**, Sample pictures of the BEC after expansion containing 0, 1, 2 and 3 solitons (**b**–**e**) or even more complex structures with bendings and crossings (**f**,**g**). For each picture, the integrated profiles of the central region are shown in black and compared to the parabolic Thomas–Fermi fit in red.

A key point of our analysis is that the number of defects that we observe is larger when the quench is faster (Fig. 2). This is a clear indication that our solitons are produced through the KZM. To provide a quantitative support to this scenario we need to check whether, for a given quench time, the transition front propagates faster than the causal horizon hence activating the KZM (ref. 18). To this end, the details of the trapping potential and the evaporation procedure are relevant. Sodium atoms are trapped in an elongated magnetic potential, whose profile is sketched in Fig. 3a (Methods). The evaporation threshold is set by a radiofrequency, of frequency $\nu_{RF}$, tuned to flip the atomic spin, from the trapped to the untrapped state, at a given potential energy from the bottom of the trap. The effective evaporation threshold is governed by the radial motion of the atoms and depends on $z$, being fixed by the difference between the evaporation threshold at the trap bottom ($r = z = 0$) and the local axial potential $U(r = 0, z)$. Moreover, the elastic collisional rate can be large enough to ensure local thermal equilibrium (collisional regime) but with a temperature gradient along the axial direction. (The axial collisional regime follows from a collisional rate typically larger than the axial trapping frequency. For instance, at the trap centre the collisional time is about 7 ms, to be compared with the axial oscillation period of 83 ms.) For these reasons, we define an axial temperature $T(z)$ as:

$$T(z) = \frac{h\nu_{RF} - U(r=0,z)}{\eta\, k_B}$$

with the truncation parameter $\eta$ of the order of 5 in our case[36]. Calculated temperature profiles for three values of evaporation radiofrequency are shown in the top panel of Fig. 3b (red dashed lines).

The cooling process starts with a ramp of radiofrequency-forced evaporation down to a temperature 10% higher than the largest critical value for observing a condensate fraction in our sample (Fig. 3c). At this stage the gas is non-condensed and in thermal equilibrium. We can estimate the profile of the critical temperature $T_c(z)$ by inserting the above-$T_c$ equilibrium density distribution of the cloud in the expression of $T_c$ for non-interacting particles:

$$T_c(z) = \frac{2\pi\hbar^2}{mk_B}\left(\frac{n(r=0,z)}{\zeta(3/2)}\right)^{2/3}$$

where $m$ is the atom mass and $\zeta(\cdots)$ the Riemann $\zeta$-function. A typical result is shown in the top panel of Fig. 3b (solid blue line) for a sample of $25 \times 10^6$ atoms. Then the system is thermally quenched by linearly reducing the evaporation threshold down to a value that ensures $T(z) < T_c(z)$ everywhere. During this process, the local temperature profile crosses the local critical temperature profile at some values of $z$, which define the positions of the BEC planar transition fronts propagating along $z$ as the temperature lowers. The speed of the transition fronts depends on $z$ and on the quench time $\tau_Q$. The latter can be varied by keeping the initial and final radiofrequencies fixed, but changing the duration of the evaporation process (Fig. 3c and Methods). The evaporation ends with a final slow ramp followed by an equilibration time (both lasting 100 ms).

The speed of a transition front can be estimated from the curves of $T(z)$ and $T_c(z)$, as those plotted in the top panel of Fig. 3b. For the speed of the causal horizon, that is, the fastest speed at which the information about the choice of a local macroscopic phase of a BEC can travel across the gas, we take the speed of sound $v_s$ (sonic horizon). A precise determination of this quantity in the vicinity of the transition and for a non-uniform gas is highly non-trivial. As a reasonable estimate we can use the expression for the sound speed derived in ref. 37 within a two-fluid model; near $T_c$, it gives $v_s^2(T) = (5\zeta(5/2)/3\zeta(3/2))k_B T + 2gn$, where $g$ is the interaction parameter related to the $s$-wave scattering length $a$ by $g = 4\pi\hbar^2 a/m$. The bottom panel in Fig. 3b shows the comparison between the speed of the transition front for different quench times (dashed lines) and the local sound speed in the gas $v_s(z) \propto \sqrt{T_c(z)}$ when neglecting interactions, which is a good approximation in our case and, more generally, for weakly interacting gases (solid line). The figure shows that indeed there are regions where the transition front moves faster than the sonic causal horizon and that the spatial extension of those regions depends on the quench time.

For given experimental conditions the number of defects we observe varies from shot to shot, as expected from the stochastic nature of the KZM. We do a quantitative characterization by counting the number of solitons observed over a large number of realizations $N_{meas}$ (Methods). The normalized statistical probability of detecting a given number of solitons, which we report in Fig. 2a for 0–5 counts and four different quench times, follows the Poissonian distribution. Figure 2b,c shows lin–lin and log–log plots of the average number of detected solitons over more than one decade in $\tau_Q$. Results are shown for two sets of measurements done with a high ($25 \times 10^6$) and low ($4 \times 10^6$) number of atoms at the transition. For each set, the vertical arrow in Fig. 2b indicates the experimentally determined quench time threshold for the observation of solitons; for larger values of $\tau_Q$, solitons are never observed in our sample. For lower values of $\tau_Q$, the average number of solitons exhibits

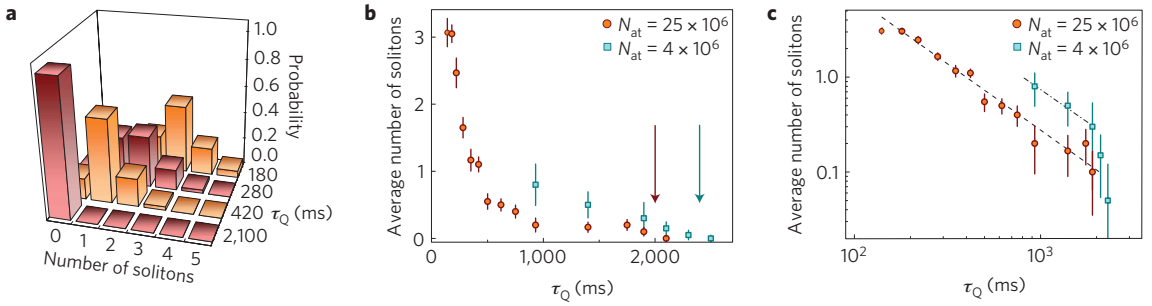


**Figure 2 | Soliton number versus quench time. a**, Counting statistics of the number of solitons observed in each shot for four different quench times $\tau_Q$ and for the data set with 25 million atoms at $T_c$. **b**,**c**, Lin–lin (**b**) and log–log (**c**) plots of the average soliton number observed as a function of $\tau_Q$. Red circles and blue squares correspond to series of data taken with different atom numbers $N_{at}$ at $T_c$, respectively 25±5 and 4±1 million. Arrows in **b** indicate the threshold in $\tau_Q$ above which solitons were never observed. The black dashed line in **c** shows the power-law dependence with exponent $-1.38 \pm 0.06$ resulting from the best fit with the data points, excluding the point at the fastest quench. The dot-dashed line with the same slope, but shifted on the second data set, serves as a guide to the eye to compare the two data sets. Reported error bars include the standard deviation of the average counts, and the resolution limit $1/N_{meas}$ added in quadrature.

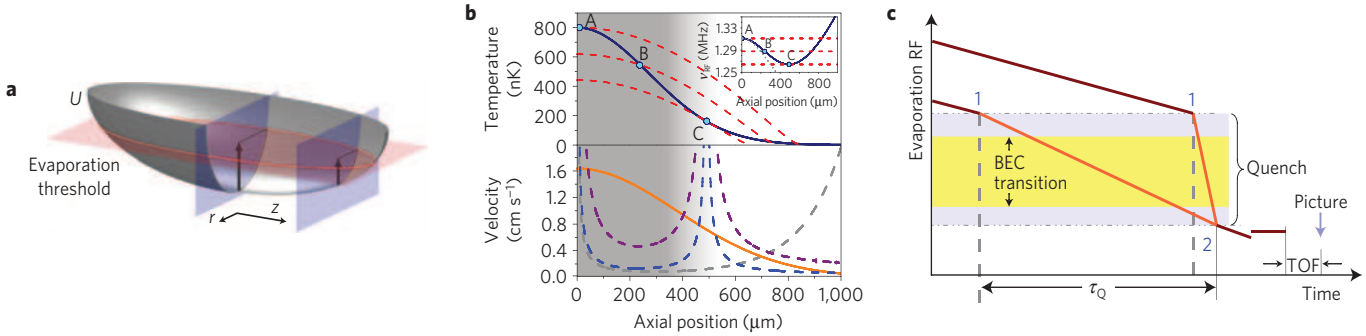


**Figure 3 | Quenched evaporation in an inhomogeneous trapped gases. a**, Sketch of the trapping potential showing the elongated weakly confined direction, $z$, and the radial tightly confined one, $r$, and the evaporation threshold set by the radiofrequency (RF) field (horizontal plane). This is reduced quickly in time so that, during the quench, atoms thermalize only radially, according to the local potential depth (see different vertical planes), giving rise to a local temperature $T(z)$. The inhomogeneous density distribution also causes a local critical temperature $T_c(z)$. **b**, The top graph shows $T_c(z)$ (solid blue line) and three different temperature profiles (dashed red) corresponding to different evaporation thresholds. During quenched evaporation condensation is first reached at the trap centre (A); then the critical point shifts towards outer regions (B and C). The inset shows the critical frequency along $z$. The lower graph shows the local sound velocity (solid orange), the local speed of the transition front for two values of $\tau_Q$ (dashed blue: 700 ms, dashed pink: 200 ms), and the front speed in the case of a uniform temperature profile (dashed grey). The comparison between these curves is meaningful where the atomic density is large (grey-shaded region). **c**, Experimental sequence. The first part of evaporation is always the same from a hot sample to a cold one above $T_c$; then a ramp with variable quench time brings the system from above to below $T_c$ (light blue regions); a short final cooling ramp allows one to increase the condensate atom number and 100 ms are left to equilibrate the system in the trap. The yellow frequency band corresponds to the extended region in which $T_c$ is crossed in the system (Methods). Atoms are then imaged after 180 ms of TOF.

a power-law dependence on $\tau_Q$ as expected for the KZM. For all points in Fig. 2 the atom loss at the end of the evaporation ramp is sufficiently small, so that the axial size of the system is the same in the whole range of $\tau_Q$ and the number of solitons and their density differ only by a constant factor. For the data set with a higher atom number and for $\tau_Q$ shorter than 140 ms, the generation of solitons is accompanied by a marked loss of atoms, hence resulting in a significant reduction of the radius of the final condensate. For smaller condensates this constraint in $\tau_Q$ is stronger, reducing the accessible range for testing the KZM. The capability of producing large condensates is thus crucial for this type of experiment.

The dashed line in Fig. 2c is the power law $\tau_Q^{-\alpha}$ with $\alpha = 1.38 \pm 0.06$ obtained by fitting the experimental data with higher $N_{at}$. This result can be compared to the prediction $\alpha = 7/6$ given in ref. 18 for the formation of grey solitons in a cigar-shaped condensate, obtained by using the critical exponent of the correlation length measured in ref. 27 and assuming the BEC transition to be in the same universality class as the superfluid transition in $^4$He (mean-field theory would instead give $\alpha = 1$). The order of magnitude is the same, but the comparison should be considered with care. The calculation in ref. 18 assumed a uniform temperature in the gas, whereas in our experimental conditions $T(z)$ is non-uniform. The difference can be appreciated by looking at the lower panel of Fig. 3b, where the speed of the transition front for the case of a uniform temperature is shown as the lower grey dashed line and compared with the local speed of sound. As one can see, the front speed is larger than the sound speed only in a narrow region near the centre of the atomic distribution, where the defects can nucleate at the transition (in the outer part of the cloud, the front is also faster than sound, but the density is vanishingly small). Conversely, with a non-uniform temperature profile, solitons can form in a wider region whose extension increases as the quench time is reduced; this may favour the observation of a larger number of solitons and may also affect the value of $\alpha$.

Further arguments supporting the interpretation of our observations in terms of the KZM come from the comparison between the two data sets with a higher and a lower atom number in Fig. 2, which leads to three main observations: the points at smaller $\tau_Q$ in the second series seem to follow the same power-law scaling of the first; the threshold for the detection of solitons is shifted towards

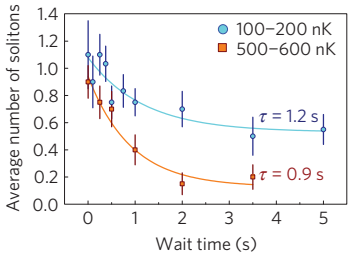


**Figure 4 | Soliton number decay.** Blue circles correspond to a very cold sample, with a barely visible thermal fraction ($T \simeq 100$–$200$ nK), whereas red squares were acquired for a hotter sample, close to $T_c$ ($T \simeq 500$–$600$ nK). The solid lines show the exponential fit to the decay. $\tau_Q = 467$ ms and $T_c \simeq 800$ nK for both data sets. The temperature is independent of the wait time. Error bars are the standard deviation of a statistical sample of 20 experimental runs.

larger $\tau_Q$ in the case of a lower atom number; for a given $\tau_Q$, the average number of solitons is larger in the case of a smaller atom number. The first observation suggests a universal behaviour, but some caution must be used here, because the smallest condensate does not allow for a reliable fit owing to the limited range of $\tau_Q$ available, as well as to the occurrence of a rather abrupt change of slope at large $\tau_Q$ (we note that change of slope and threshold phenomena in KZM were also discussed in refs 25,26,38,39 for other systems). The second observation is consistent with the fact that a smaller atom number at $T_c$ implies a lower sound speed and hence defects can be created for slower quenches (larger $\tau_Q$), as we indeed observe. Using the expression from ref. 37 for the sound speed, near $T_c$ one gets approximately $v_s \propto \sqrt{T_c} \propto N_{at}^{1/6}$. Thus, in the case of a lower atom number the sound speed at $T_c$ is smaller by a factor $0.74 \pm 0.06$. The positions of the two arrows indicating the thresholds in Fig. 2b differ by a factor $0.84 \pm 0.08$ in the right direction and in reasonable agreement with expectations. A quantitative comparison between the two data sets, however, would require a better theoretical understanding of threshold phenomena in finite inhomogeneous systems. The third observation is again consistent with the KZM in the sense that a slower sonic horizon, at fixed quench time, increases both the size of the region where the transition front is supersonic and the soliton density, yielding a shift of the scaling law upwards in the log–log plot.

We finally discuss the possible spurious effects that may alter the counting of solitons, hence modifying the data in Fig. 2. We already mentioned that, in the limit of very fast quenches, the efficiency of the evaporative cooling drops causing additional atom losses at the transition and in the final condensate. The point at $\tau_Q = 140$ ms lies in a range where these effects may start being relevant. On the other hand, when a slow quench is applied, one may wonder whether solitons decay before being observed. To address this question, in Fig. 4 we report the average number of solitons observed in the condensate as a function of the time spent in-trap after an intermediate evaporation quench time. Two sets of data are collected for different values of the temperature after the evaporation. In both sets, the number of solitons shows a decay with a tendency to saturate to a finite value for long times. The decay is faster when the temperature is larger, consistent with the idea that, at finite $T$, grey solitons are accelerated towards the edges of the cloud where they can dissipate their energy into thermal excitations (this decay mechanism has recently been observed in a superfluid Fermi gas[40]). If $T \ll T_c$, in the worst case of a wait time of 2 s, the counts drop only by about 30%, which is a reasonably small loss when compared with the error bars of Fig. 2. The tendency to saturate at a finite value suggests that a sizable fraction of solitons has a much longer lifetime. This can be explained in terms of the generation of solitons near the centre of the trap with a small initial velocity. These solitons can oscillate back and forth for very long times before dissipating their energy.

In combination with the observations of ref. 23, our results should stimulate the study of the interplay between the inhomogeneous and homogeneous KZM (ref. 20). In addition, an extension of the theory of ref. 18 to the case of non-uniform temperature profiles could allow one to extract from our observations the values of the critical exponents for BEC in dilute gases.

## Methods

**Sample preparation.** A high-flux beam of cold sodium atoms is produced in a compact system based on a short Zeeman slowing stage and on a coplanar two-dimensional magneto-optical trap[41]. The bright atomic beam fills a three-dimensional dark-spot magneto-optical trap in 8 s. A few-millisecond dark-spot molasses phase helps to increase the phase space density to $3 \times 10^{-6}$ and improve the transfer efficiency into the magnetic trap. Our magnetic trap has a Ioffe–Pritchard[42] geometry with final axial and radial trapping frequencies of $\omega_z = 2\pi \times 12$ Hz and $\omega_r = 2\pi \times 119$ Hz. Starting with $10^9$ atoms in the magnetic trap we cool them by means of a Zeeman-forced evaporation with a two-step ramp, first reducing the radiofrequency at 1.2 MHz s$^{-1}$ for 30 s, then the trap is decompressed by a factor $\sqrt{2}$ to the final trapping frequencies and evaporation continues at 190 kHz s$^{-1}$ for 8 s. At the end of the preparation stage the atomic sample contains $25 \times 10^6$ atoms just above $T_c$. The trapping potential has a cigar shape horizontally oriented along $z$.

**Temperature quench.** As illustrated in Fig. 3c we explore the KZM by crossing the BEC transition point with different evaporation quench rates. The starting point is always 1.39 MHz, 190 kHz above the trap bottom. The BEC transition frequency is not unique. To make sure that the BEC transition is always crossed throughout the whole sample during the quench we need to take several effects into account: the density inhomogeneity across the sample introduces a transition frequency interval; changing the quench rate slightly shifts the transition point because of the different amount of removed atoms; technical shot-to-shot atom number fluctuation also shifts the transition point. For all of these reasons we set a fixed frequency band from 1.39 MHz to 1.25 MHz, within which the whole sample crosses the BEC transition for any given experimental quench rate. The quench time $\tau_Q$ reported in the text is defined as the time interval employed to perform this linear quench ramp of 140 kHz. The quench is followed by a 100-ms-long further evaporation at 300 kHz s$^{-2}$ down to 1.22 MHz, to maximize the condensate fraction, and a final 100 ms during which the radiofrequency is kept fixed at 1.24 MHz allowing for solitons stabilization and evolution.

**Levitation.** On switching off the elongated magnetic trapping potential the chemical potential is suddenly transferred into kinetic energy and atoms mainly expand along the tightly confined radial direction assuming a spherical shape after about 15 ms; then the atomic distribution becomes pancake-like. In the meantime, the sample would naturally fall under gravity and reach the glass vacuum cell within 50 ms time. To avoid this and allow for longer expansion times to observe atoms without optical density saturation, we levitate the sample by switching on just one of the two quadrupole coils producing a vertical gradient of the magnetic field modulus, able to compensate the gravitational force for atoms in $|F = 1, m_F = -1\rangle$. The residual magnetic field curvature in the horizontal plane gives rise to a negligible trapping effect.

**Imaging.** The least energetic and most stable orientation for solitons in an elongated BEC is the one orthogonal to the trap symmetry axis. Density depletion can be therefore observed by looking along any radial direction. We image the condensates along two orthogonal directions in the radial plane to minimize underestimating soliton counts owing to any possible residual tilt of the solitonic plane. Absorption imaging is performed after a levitation time of 180 ms. In this way, the optical density of the condensate is of the order of 1 or smaller, no saturation is present and density variations in the sample are clearly visible. Atoms are imaged using light resonant with the $|F = 2\rangle \rightarrow |F' = 3\rangle$ transition. As atoms are magnetically trapped in $|F = 1, m_F = -1\rangle$, repumping light tuned on the $|F = 1\rangle \rightarrow |F' = 2\rangle$ transition is needed to pump them in $|F = 2\rangle$. A thin light-sheet (waist of 600 μm) propagating along the vertical direction is used to repump only a central region of the expanded condensate (Thomas–Fermi radius of 2.5 mm) to further reduce optical density and increase the soliton contrast.

**Data analysis.** For each set of experimental parameters, such as temperature, quench time and atom number at the transition, the experiment was repeated 20–40 times (depending on the resulting average number of solitons observed) to minimize the error bars in Fig. 2. The number of solitons visible in each image was counted (Fig. 1b–e) and the average number was plotted for any given set of parameters. Error bars include the standard deviation of the average counts, and the resolution limit $1/N_{meas}$ added in quadrature.

Received 25 April 2013; accepted 25 July 2013; published online 8 September 2013; corrected online 19 September 2013

## References


1. Kibble, T. W. B. Topology of cosmic domains and strings. *J. Phys. A* **9,** 1387 (1976).
2. Kibble, T. Some implications of a cosmological phase transition. *Phys. Rep.* **67,** 183–199 (1980).
3. Zurek, W. H. Cosmological experiments in superfluid liquid helium? *Nature* **317,** 505–508 (1985).
4. Zurek, W. Cosmological experiments in condensed matter systems. *Phys. Rep.* **276,** 177–221 (1996).
5. Del Campo, A., Kibble, T. W. B. & Zurek, W. H. Causality and non equilibrium second-order phase transitions in inhomogeneous systems. Preprint at http://arxiv.org/abs/1302.3648v1 (2013).
6. Dziarmaga, J., Smerzi, A., Zurek, W. H. & Bishop, A. R. Dynamics of quantum phase transition in an array of Josephson junctions. *Phys. Rev. Lett.* **88,** 167001 (2002).
7. Zurek, W. H., Dorner, U. & Zoller, P. Dynamics of a quantum phase transition. *Phys. Rev. Lett.* **95,** 105701 (2005).
8. Bäuerle, C., Bunkov, Y. M., Fisher, S. N., Godfrin, H. & Pickett, G. R. Laboratory simulation of cosmic string formation in the early Universe using superfluid $^3$He. *Nature* **382,** 332–334 (1996).
9. Ruutu, V. M. H. *et al.* Vortex formation in neutron irradiated $^3$He as an analogue of cosmological defect formation. *Nature* **382,** 334–336 (1996).
10. Carmi, R. & Polturak, E. Search for spontaneous nucleation of magnetic flux during rapid cooling of $YBa_2Cu_3O_{7-\delta}$ films through $T_c$. *Phys. Rev. B* **60,** 7595–7600 (1999).
11. Carmi, R., Polturak, E. & Koren, G. Observation of spontaneous flux generation in a multi-Josephson-junction loop. *Phys. Rev. Lett.* **84,** 4966–4969 (2000).
12. Monaco, R., Mygind, J. & Rivers, R. J. Zurek–Kibble domain structures: The dynamics of spontaneous vortex formation in annular Josephson tunnel junctions. *Phys. Rev. Lett.* **89,** 080603 (2002).
13. Monaco, R., Mygind, J. & Rivers, R. J. Spontaneous fluxon formation in annular Josephson tunnel junctions. *Phys. Rev. B* **67,** 104506 (2003).
14. Monaco, R., Mygind, J., Rivers, R. J. & Koshelets, V. P. Spontaneous fluxoid formation in superconducting loops. *Phys. Rev. B* **80,** 180501 (2009).
15. Pyka, K. *et al.* Symmetry breaking and topological defect formation in ion coulomb crystals. *Nature Commun.* **4,** 2291 (2012).
16. Ulm, S. *et al.* Observation of the Kibble–Zurek scaling law for defect formation in ion crystals. *Nature Commun.* **4,** 2290 (2013).
17. Ejtemaee, S. & Haljan, P. C. Spontaneous nucleation and dynamics of kink defects in zigzag arrays of trapped ions. *Phys. Rev. A* **87,** 051401 (2013).
18. Zurek, W. H. Causality in condensates: Gray solitons as relics of BEC formation. *Phys. Rev. Lett.* **102,** 105702 (2009).
19. Damski, B. & Zurek, W. H. Soliton creation during a Bose–Einstein condensation. *Phys. Rev. Lett.* **104,** 160404 (2010).
20. Del Campo, A., Retzker, A. & Plenio, M. B. The inhomogeneous Kibble–Zurek mechanism: Vortex nucleation during Bose–Einstein condensation. *J. Phys.* **13,** 083022 (2011).
21. Witkowska, E., Deuar, P., Gajda, M. & Rzą zewski, K. Solitons as the early stage of quasicondensate formation during evaporative cooling. *Phys. Rev. Lett.* **106,** 135301 (2011).
22. Sabbatini, J., Zurek, W. H. & Davis, M. J. Phase separation and pattern formation in a binary Bose–Einstein condensate. *Phys. Rev. Lett.* **107,** 230402 (2011).
23. Weiler, C. N. *et al.* Spontaneous vortices in the formation of Bose–Einstein condensates. *Nature* **455,** 948–952 (2008).
24. Chen, D., White, M., Borries, C. & DeMarco, B. Quantum quench of an atomic Mott insulator. *Phys. Rev. Lett.* **106,** 235304 (2011).
25. Dziarmaga, J., Tylutki, M. & Zurek, W. H. Quench from Mott insulator to superfluid. *Phys. Rev. B* **86,** 144521 (2012).
26. Del Campo, A., De Chiara, G., Morigi, G., Plenio, M. B. & Retzker, A. Structural defects in ion chains by quenching the external potential: The inhomogeneous Kibble–Zurek mechanism. *Phys. Rev. Lett.* **105,** 075701 (2010).
27. Donner, T. *et al.* Critical behavior of a trapped interacting Bose gas. *Science* **315,** 1556–1558 (2007).
28. Burger, S. *et al.* Dark solitons in Bose–Einstein condensates. *Phys. Rev. Lett.* **83,** 5198–5201 (1999).
29. Denschlag, J. *et al.* Generating solitons by phase engineering of a Bose–Einstein condensate. *Science* **287,** 97–101 (2000).
30. Becker, C. *et al.* Oscillations and interactions of dark and dark-bright solitons in Bose–Einstein condensates. *Nature Phys.* **4,** 496–501 (2008).
31. Chang, J. J., Engels, P. & Hoefer, M. A. Formation of dispersive shock waves by merging and splitting Bose–Einstein condensates. *Phys. Rev. Lett.* **101,** 170404 (2008).
32. Shomroni, I., Lahoud, E., Levy, S. & Steinhauer, J. Evidence for an oscillating soliton/vortex ring by density engineering of a Bose–Einstein condensate. *Nature Phys.* **5,** 193–197 (2009).
33. Anderson, B. P. *et al.* Watching dark solitons decay into vortex rings in a Bose–Einstein condensate. *Phys. Rev. Lett.* **86,** 2926–2929 (2001).
34. Carr, L. D. & Brand, J. in *Emergent Nonlinear Phenomena in Bose–Einstein Condensates: Theory and Experiment* (eds Kevrekidis, P. G., Frantzeskakis, D. J. & Carretero-Gonzalez, R.) Ch. 7 (Springer, 2009).
35. Dalfovo, F. & Modugno, M. Free expansion of Bose–Einstein condensates with quantized vortices. *Phys. Rev. A* **61,** 023605 (2000).
36. Ketterle, W. & van Druten, N. in *Advances in Atomic, Molecular, and Optical Physics* 37 (eds Bederson, B. & Walther, H.) 181–236 (1996).
37. Hu, H., Taylor, E., Liu, X-J., Stringari, S. & Griffin, A. Second sound and the density response function in uniform superfluid atomic gases. *New J. Phys.* **12,** 043040 (2010).
38. Weir, D. J., Monaco, R., Koshelets, V. P., Mygind, J. & Rivers, R. J. Gaussianity revisited: Exploring the Kibble–Zurek mechanism with superconducting rings *J. Phys. Condens. Matter* Preprint at http://arxiv.org/abs/1302.7296v2 (2013).
39. Su, S-W., Gou, S-C., Bradley, A., Fialko, O. & Brand, J. Kibble–Zurek scaling and its breakdown for spontaneous generation of Josephson vortices in Bose–Einstein condensates. *Phys. Rev. Lett.* **110,** 215302 (2013).
40. Yefsah, T. *et al.* Heavy solitons in a fermionic superfluid. *Nature* **499,** 426–430 (2013).
41. Lamporesi, G., Donadello, S., Serafini, S. & Ferrari, G. Compact high-flux source of cold sodium atoms. *Rev. Sci. Instrum.* **84,** 063102 (2013).
42. Pritchard, D. E. Cooling neutral atoms in a magnetic trap for precision spectroscopy. *Phys. Rev. Lett.* **51,** 1336–1339 (1983).


## Acknowledgements

We are indebted to L. P. Pitaevskii, I. Carusotto and A. Recati for fruitful discussions. This work is supported by Provincia Autonoma di Trento.

## Author contributions

G.L., S.D., S.S. and G.F. built the experimental set-up; G.L., S.D. and G.F. performed data acquisition; G.L. and G.F. analysed the data; all authors contributed to the discussion of the results and G.L., S.D., F.D. and G.F. participated in manuscript preparation.

## Additional information

Reprints and permissions information is available online at www.nature.com/reprints. Correspondence and requests for materials should be addressed to G.F.

## Competing financial interests

The authors declare no competing financial interests.

ERRATUM

# Spontaneous creation of Kibble–Zurek solitons in a Bose–Einstein condensate

Giacomo Lamporesi, Simone Donadello, Simone Serafini, Franco Dalfovo and Gabriele Ferrari

*Nature Physics* http://dx.doi.org/10.1038/nphys2734 (2013); published online 8 September 2013; corrected online 19 September 2013.

In the version of this Article originally published online, in Fig. 2b,c, the values of $N_{at}$ for each data series were missing from the legend. This error has now been corrected in all versions of the Article.